Sensor and Simulation Notes

Note 528

May 2008

An Electromagnetic Analysis Of The 46cm Diameter Impulse Radiating Antenna (IRA)

Mary C. Taylor and Tapan K. Sarkar

Syracuse University
Electrical Engineering and Computer Science Department
Syracuse, New York 13244

Abstract

An impulse radiating antenna has been built by E. Farr and his associates and has been in operation for some time [1-7]. The objective of this document is to illustrate that it is possible to duplicate the measured results both in the time and frequency domain of the electrical characteristics of the antenna using an electromagnetic analysis code. The electromagnetic analysis code used to analyze the structure in the frequency domain is the antenna analysis computer program called WIPL-D [8]. Since this code uses entire domain basis functions over large subsectional patches it is possible to analyze electrically large structures on desktop computers utilizing modest computational resources. The greatest advantage of being able to analyze practical antennas using electromagnetic analysis codes is that the structure can be optimized in a cost effective fashion using modest computational resources as opposed to using super computers and an elaborate measurement campaign which often becomes quite costly and time consuming. The goals of the analysis are summarized as:

1. Modeling and simulation of the 46cm diameter IRA using WIPL-D based on a Farr Research IRA with 45º feed arms.
2. Post processing of the frequency domain response of the IRA obtained by the electromagnetic analysis code WIPL-D into time domain by weighting the frequency domain response by a Gaussian window and using inverse discrete Fourier transform (IDFT) through Matlab.
3. Integration of the time domain response so as to obtain the step response of the IRA and compare it with the experimental results obtained by Farr research. The derivative relationship between the far field time domain transmission and reception is also shown.
4. Integration of the time domain response of the impedance data resulting in an equivalent response that would be obtained by a time domain reflectometer (TDR).

In addition, we compare simulated IRA beam patterns for nine frequencies and present plots which support the selection of 200Ω for the load resistor based on simulations of six different resistor values.

PHYSICAL DESCRIPTION OF THE IRA MODEL THAT WILL BE USED FOR ANALYSIS:

The dimensions of the IRA-2 were supplied by E. Farr [3], and this document is provided in the Appendix for reference. The structure is a 46cm diameter IRA for which the electromagnetic response has been measured up to 20 GHz. Here we provide an electromagnetic analysis and illustrate that for this IRA it is possible to carryout an efficient, accurate, detailed analysis of the antenna structure. We can further optimize the IRA structure for best performance. One of the important points of this analysis is that it is not necessary to carry out repeated computations as the results obtained from this computer code are quite accurate and yield the right results the first time. The advantage of using the code WIPL-D is that it uses higher order basis functions over large quadrilateral patches. Typically, if one were to use subsectional basis functions like the triangular patches used in [5], then typically one needs roughly 300 unknowns to represent the unknown currents numerically over a one square wavelength of the surface area. However, for WIPL-D we use entire domain polynomial basis functions over large quadrilateral patches and therefore we need only 10-20 unknowns to characterize the same unknown current over a square wavelength of surface area. This results in a reduction in the number of unknowns at least by a factor of 10 over the use of conventional piecewise subsectional bases. Therefore, problems which require super computers to solve using the subsectional triangular patch basis functions can be solved on a desktop computer using WIPL-D resulting in significant efficiency. In addition, since we are using entire domain basis functions in WIPL-D, the continuity of the charge is guaranteed and therefore WIPL-D provides a more accurate result for the near field and hence the input impedance. This produces a much faster rate of convergence for the results related to the parameter of interest.

TABLE 1: List of symbols used to describe the parameters of the IRA

| Symbol	[meters]	Parameter	Description
D	0.46	given	Diameter of the Paraboloidal Reflector Aperture
F/D	0.4	given	Ratio of Focal Length to Aperture Diameter [unitless]
L/D	0.4	given	Ratio of Feed Arm Sphere Radius to Aperture Diameter
		Calculated	
R	0.23	=D/2	Radius of Paraboloidal Reflector Aperture
F	0.18	=(F/D)*D	Focal Length
L	0.18	=(L/D)*D	Radius of Feed Arm Sphere
d	0.07	=R^2/(4*F)	Depth of Paraboloidal Reflector
L_a	0.26	=sqrt{(F-d)^2+R^2}	Length from Focal Point to Reflector Rim
Angle from axis	**[radians]**	**[degrees]**	
Beta_1	0.92	52.46	= acos[(F-d)/F] (also = asin[(sqrt(F^2-(F-d)^2))/F])
Beta_0	1.12	64.01	= acos[(F-d)/L $_a$] (also = asin[(R)/L $_a$])
Beta_2	1.32	75.57	= Beta_0 + Delt20
Included Angle			
Delt01	0.20	11.56	= Beta_0 - Beta_1
Delt20	0.20	11.56	= Delt01
Delt21	0.40	23.11	= Delt20 + Delt01

ELECTROMAGNETIC MODELING OF THE IRA USING WIPL-D:

In this section we present the data for a 46 cm IRA with a 45º feed arms. A parametric model has been developed in WIPL-D using the values shown in Table 1. The advantage of using a parametric representation of the structure is that it can easily be scaled for optimization. The specifications were derived from E. Farr's IRA-2 [3]. To allow for maximum scalability of the model, only 3 parameters: D, F/D and L/D, were assumed as "given" and all other values are derived from these three parameters. Some calculated values were found to differ slightly from the numbers given by the Farr document [3], yet the calculated values were used instead as it will be efficient in optimizing the structure later for a specified performance. Another difference is that the IRA-2 uses 30º feed arms, as shown in the photo below [10, Figure 3.1], and instead we used 45º feed arms for our initial modeling effort. The model can be scaled for 30º feed arms in future investigations.
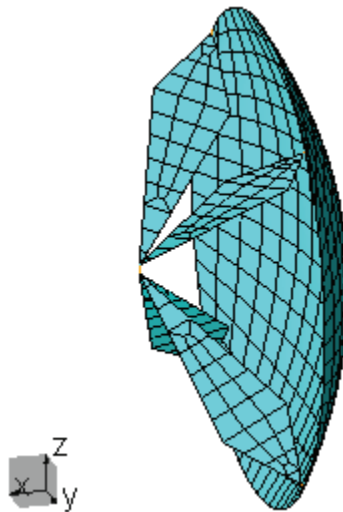

**Figure 1** a) Photo of the IRA-2 with 30º feed arms [10]

The next three figures illustrate the model that has been used for the 46 cm IRA with 45 degree feed arms.
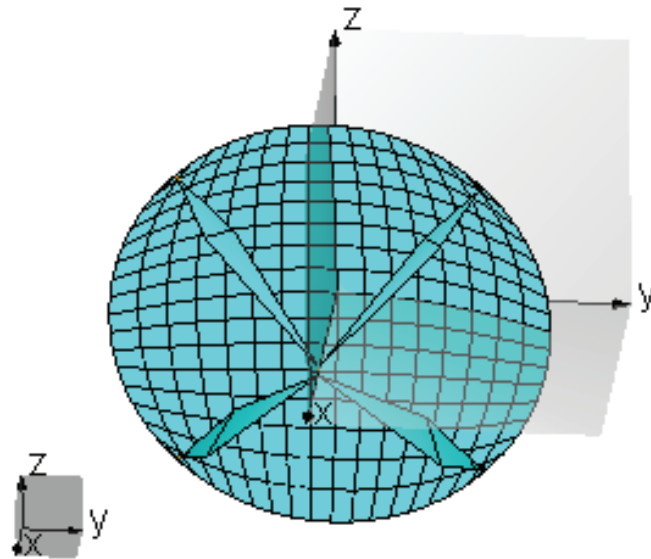
Figure 1 b) shows a model of the full IRA, with the reflector segmented using 16 subsections around the quarter of the circumference (n=16) for carrying out an accurate electromagnetic simulation up to 20GHz.


Figure 2 shows the same full IRA using quadrilateral patches in the WIPL-D segmentation, along with the feed arms for simulation up to 20GHz.
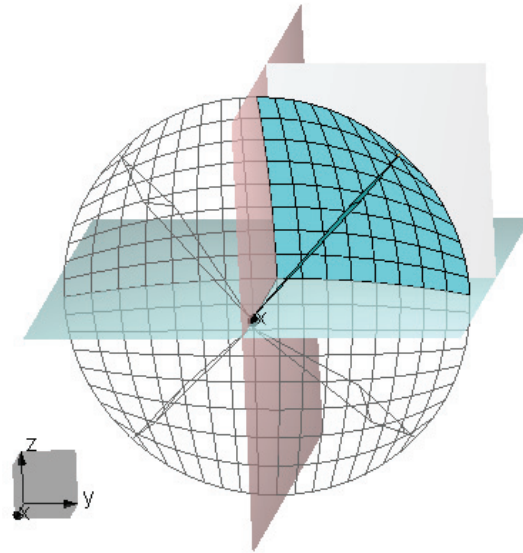
Figure 3 shows only a quarter of the IRA. Here, two planes of symmetry have been used to reduce the number of unknowns and the computer time for the simulations.

Next we zoom in to the structure to show the details. In Figures 4 through 8, we zoom in to the feed wire connecting the feed arm and the generator section of a quarter of the IRA model. The junction of the feed wire to the feed arm is also highlighted.

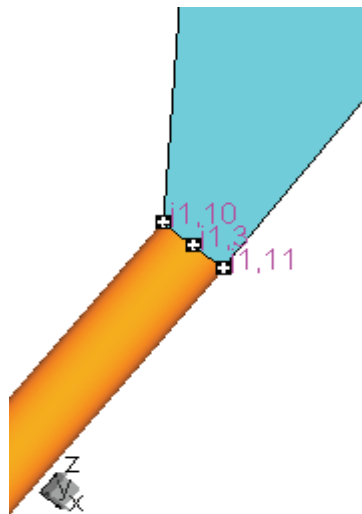Fed by delta point generator located at the tip of this conical shaped feed wire.
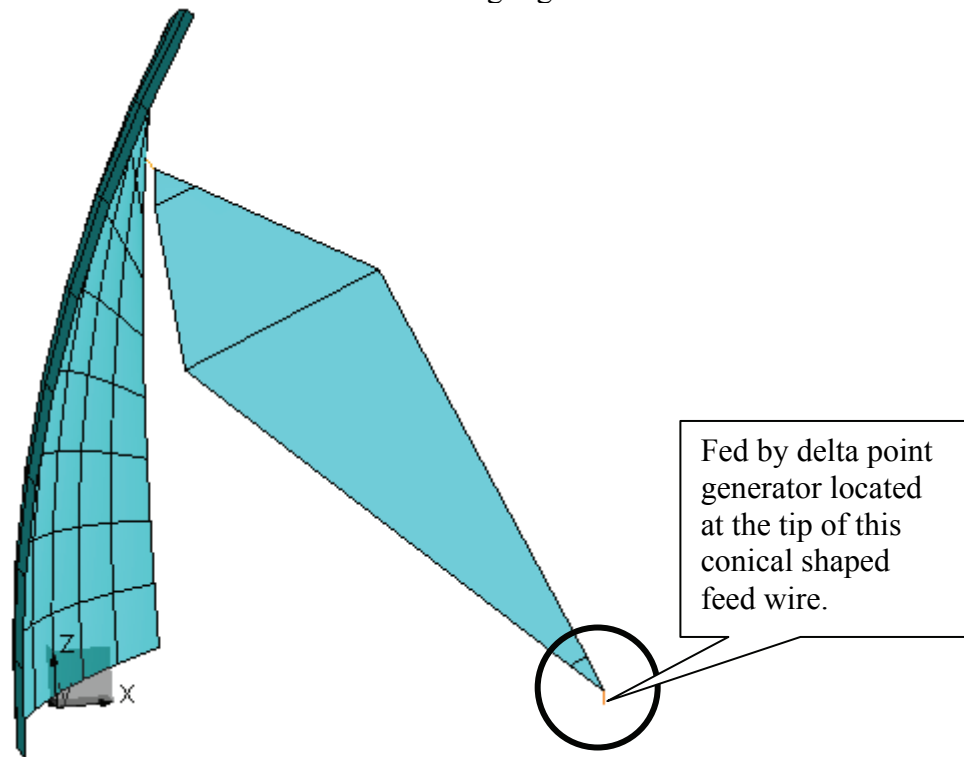
Figure 4 shows a side view of the quarter of the IRA with the feed area circled.
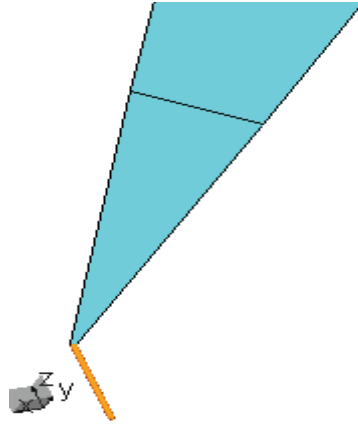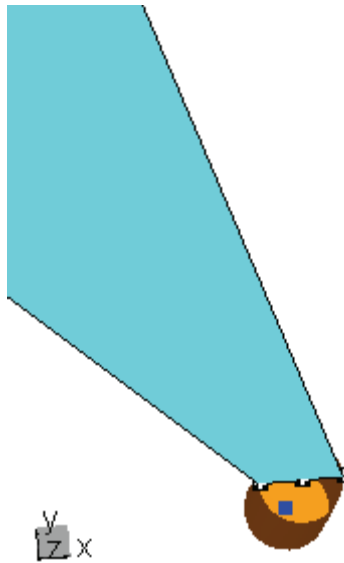
Figure 5 zooms in on the feed wire and junction of this wire to the first plate that forms the feed arm.

Figure 6 shows the generator connected to the conical feed wire containing the generator.


Figure 7 displays the junction between the feed wire and the first plate of the feed arm.

Figure 8 is a top view looking into the end of the feed wire connected to the feed arm. The generator (dark blue) can be seen from inside the feed wire, at the center of the conical wire.

Next, we zoom in on the connection between the feed arm and the reflector as shown in Figure 9. Figure 10 shows the connecting load resistance.
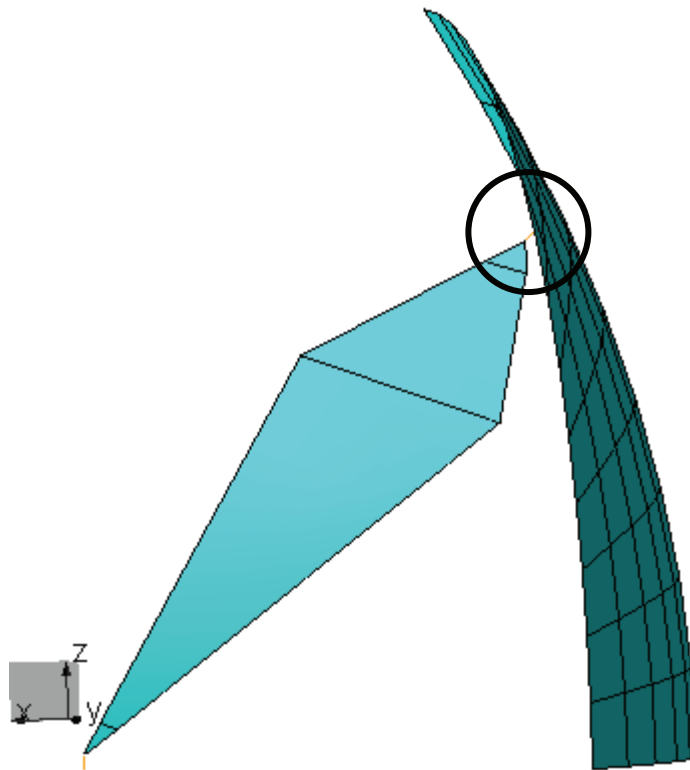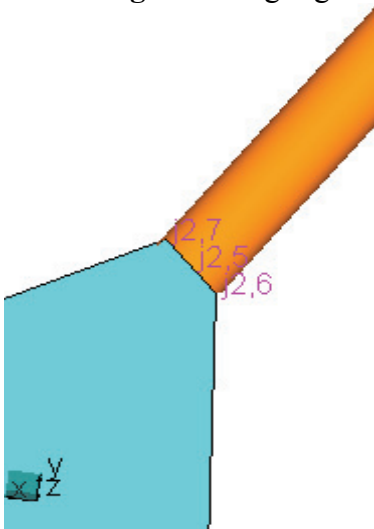

Figure 9 shows a side view of the quarter of the IRA. The connection between the feed arm and the reflector has been circled.
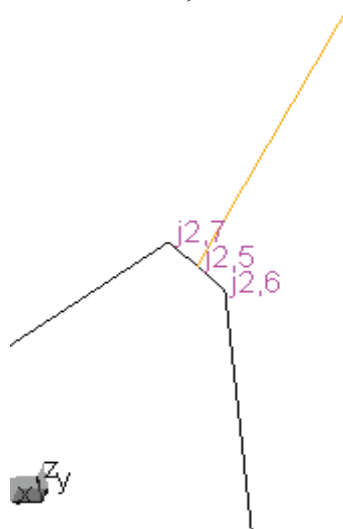
Figure 10 shows the connection of the feed arm to the reflector surface. Figures 11-13 zoom in on this connection.
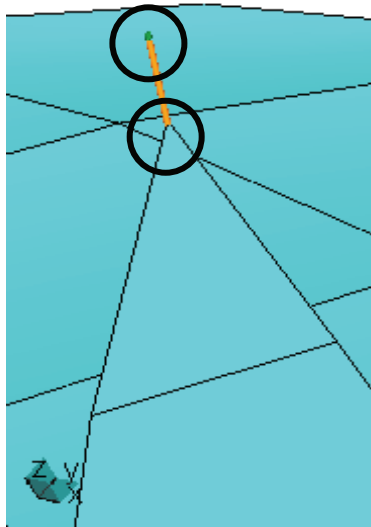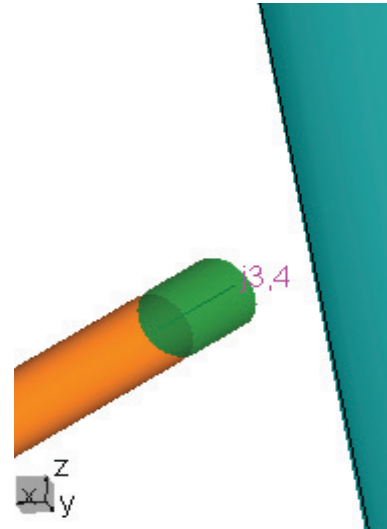

Figure 10 highlights the connection area, with the two ends of the wire circled.

Figure 11   **Figure 12**   **Figure 13**

Figure 11 zooms in on the junction from the plate to the connecting wire.
Figure 12 shows the same junction, without the shading, to highlight the quadrilateral shape of the plate edge.
Figure 13 zooms in on the wire end connected to the concentrated load and then to the reflector.

The data for these plots are represented symbolically in WIPL-D so that one can simply change the shape or the size of the IRA by changing the values in the symbol list of WIPL-D. The user does not have to discretize the structure into quadrilaterals as that is automatically done by the computer code. The list of symbols is provided in Figure 14. Figure 15 provides the lists of plates, wires and generators that make up the electrical model of the IRA.

#	Value	Symbol
1	200	load=200
2	39.36	inperm=39.36
3	3.14159	pi=3.14159
4	0.46	D_m=.46
5	18.1056	D_in=D_m*inperm
6	0.46	D=D_m
7	0.23	R=D/2
8	0.4	FoD=.4
9	0.4	LoD=FoD
10	0.184	F=FoD*D
11	0.184	L=LoD*D
12	0.071875	d=R^2/(4*F)
13	0.255875	La=(R^2+(F-d)^2)^(1/2)
14	1.25	aof=R/F
15	1.1172	B0=acos((F-d)/La)
16	0.915524	B1=acos((F-d)/L)
17	0.201674	dB=B0-B1
18	1.31887	B2=B0+dB
19	0.046	wwl=D/10
20	0.0046	wL=wwl/10
21	0.000153333	wR=wL/30
22	0.000108423	dw=wR/(2^(1/2))
23	8.85272e-05	dwL1=(wR)/(tan(pi/3))
24	7.66667e-05	dwL=wL/60
25	0.00452333	wL2=wL-dwL
26	6.52174e+09	f_res=3e8/wwl
27	0.069	patchL=1.5*wwl
28	3.33333	ptchperR=R/patchL
29	0.14589	z2=L*sin(B1)
30	0.138135	x1=F-(L*cos(B2))
31	0.178192	z3=L*sin(B2)
32	0.103371	xm=F-(L*cos(B0))
33	0.165393	zm=L*sin(B0)
34	0.183847	x1w1=F-wR
35	0.184153	x2w1=F+wR
36	0.225865	z1w2=R-(wL*sin(B0))
37	0.0738907	x1w2=d+(wL*cos(B0))
38	0.0737823	x2w2=x1w2-dw
39	0.225757	z2w2=z1w2-dw
40	0.0739992	x3w2=x1w2+dw
41	0.225974	z3w2=z1w2+dw
42	0.2116	z4=R-4*wL
43	0.21758	z5=z4+1.3*wL
44	0.085675	x5=d+3*wL
45	0.17503	x6=F-1.95*wL
46	0.015364	z6=3.34*wL
47	0.0184	z7=4*wL
48	0.18078	x7=F-0.7*wL
49	16	n=16
50	1	boa=1
51	45	theta=45
52	0.000168667	jr=wR*1.1
53	0.162635	j=R/(2^(1/2))
54	0.159382	j2=j-wL/(2^(1/2))
55	0.00122667	r=wR*8
56	0.00353846	r2=wL/1.3
57	0.158035	jw=j-wL
58	0.00325269	djw=wL/(2^(1/2))
59	0.154782	jwy=jw-djw
60	0.161287	jwz=jw+djw

Figure 14 provides the symbol list of all the parameters.

	Coordinates		
	x [m]	y [m]	z [m]
1	F	0	0
2	F	0	dwL1
3	F	0	wL
4	d	0	R
5	x1w2	0	z1w2
6	x2w2	0	z2w2
7	x3w2	0	z3w2
8	d	0	z2
9	x1	0	z3
10	x1w1	0	wL
11	x2w1	0	wL
12	d	0	z4
13	x5	0	z5
14	x6	0	z6
15	x7	0	z7
16	F	0	-dwL1
17	F	0	-wL
18	d	0	-R
19	x1w2	0	-z1w2
20	x2w2	0	-z2w2
21	x3w2	0	-z3w2
22	d	0	-z2
23	x1	0	-z3
24	x1w1	0	-wL
25	x2w1	0	-wL
26	d	0	-z4
27	x5	0	-z5
28	x6	0	-z6
29	x7	0	-z7

☐ Merge

Plates

	Nodes				Domains		Current	
	1st	2nd	3rd	4th	1st	2nd	Ncp	Ncs
1	15	14	11	10	1	0	0	0
2	9	8	15	14	1	0	1	0
3	13	9	12	8	1	0	0	0
4	7	13	6	12	1	0	0	0
5	25	24	29	28	1	0	0	0
6	23	22	29	28	1	0	0	0
7	23	27	22	26	1	0	0	0
8	21	27	20	26	1	0	0	0

Wires

	Nodes		Radii [m]		Do.	Ncs.
	1st	2nd	1st	2nd	1st	
1	1	2	0	wR	1	0
2	2	3	wR	wR	1	2
3	5	4	wR	wR	1	0
4	1	16	0	wR	1	0
5	16	17	wR	wR	1	0
6	19	18	wR	wR	1	0

Junctions

	Nodes											
	1.	2.	3.	4.	5.	6.	7.	8.	9.	10.	11.	12.
1	4	0	0	0	0	0	0	0	0	0	0	0
2	18	0	0	0	0	0	0	0	0	0	0	0

Generators

	Nodes		Voltage [V]	
	1st	2nd	Real	Imag
1	1	2	1	0

Figure 15 provides the lists of all nodes, plates, wires, junctions and the generators that make up the IRA.

USING WIPL-D TO COMPUTE THE RADIATED FIELD GENERATED BY THE IRA:

In this section, the radiation fields for the IRA are calculated in the frequency domain using WIPL-D and then the results are inverse Fourier transformed to generate the time domain response. First, the final time domain response plot is shown and explained below. Next, the frequency domain data is presented and then, the transformation to the time domain is developed and displayed.

In Figure 16 below, the blue line shows the time domain response of the IRA to a Gaussian input pulse. The IRA as a transmitting antenna thus differentiates the input impulse, producing a pulse doublet in the far field.

Therefore, if a step is applied to the IRA, it will differentiate the step producing a radiated impulsive field, as it differentiates the waveform on transmit. Since the IRA acts as a differentiator on transmit, it will differentiate the step providing an impulse in the far field. To simulate the time domain response of the IRA to a step input, we recognize that the desired step input is the integral of the impulse we used. Therefore, we take the integral of the far-field radiation pattern due to the impulse input (shown in blue), which results in the far-field radiation pattern due to a step input and is shown by the red line in Figure 16. The shape of this plot agrees with the theoretical shape of the IRA transmit impulse [9]. The initial prepulse, due to the direct radiation of the currents on the feed arms, starts at approximately 4.2nsec, and lasts for the time it takes for the initial wave to travel two times the focal length of the IRA, which is 2F/c = 1.2nsec. The actual impulse starts after the prepulse, and the tail of the impulse extends for a distance beyond the impulse. The shape of the plots in Figure 16 is reasonable, but the amplitudes have been normalized to allow all the plots to be seen together.
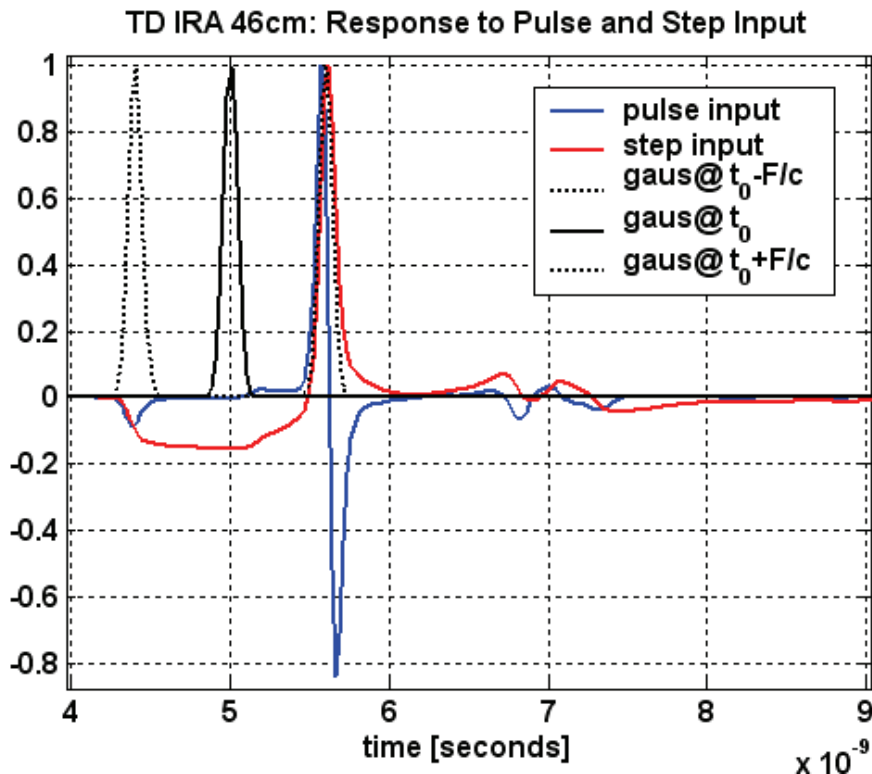

Figure 16 plots both the impulse (blue) and the step (red) response of the 46cm diameter IRA.

Also shown in Figure 16 is the shape of the Gaussian input pulse that is applied to the feed of the IRA. The impulse is displayed at three different physical locations as it propagates down the antenna feed arms. The feed point, in this model of the IRA is located in front of the origin, and the impulse is shown at three different locations of $t_0 = 5$nsec, t_0–F/c and at t_0+F/c.
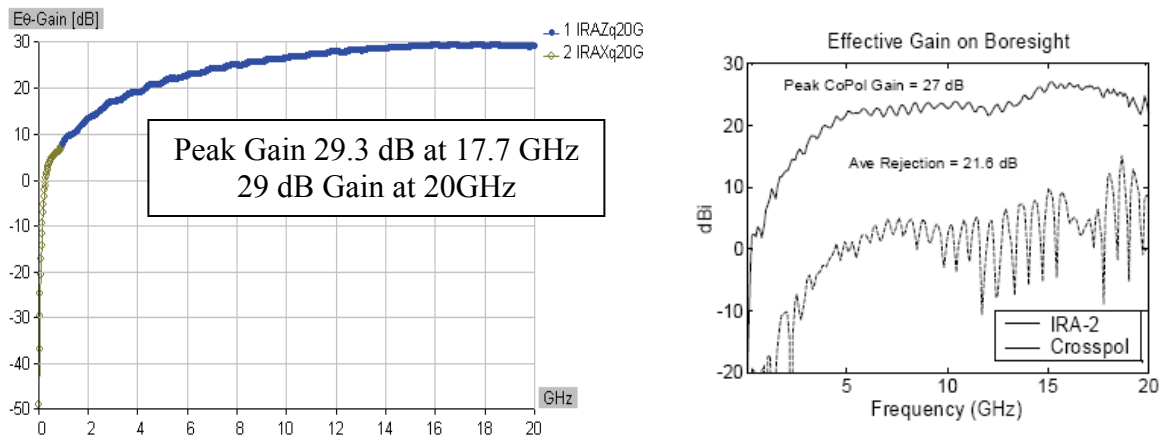
The results from the frequency domain simulation using WIPL-D are shown in Figure 17a below. This plot shows good agreement with published measurements [4, 10], with a boresight gain of almost 30dB at 20GHz. Figure 17b is a plot of IRA-2 measured data [10, Figure 3.4] for comparison.

Using the quarter symmetric model, the number of unknowns in WIPL-D was reduced from 10325 for the full model to just 2583. The frequency parameters used in the simulation are summarized below.

Start Frequency	20 MHz
Stop Frequency	20 GHz
Frequency Step	20 MHz
Number of Frequencies	1000

A 20MHz frequency step was used as a tradeoff to get as much frequency resolution as possible in a short amount of computer time. The required computer time was approximately 75 seconds per frequency, for a total of about 21 hours. The computer used was a Pentium 4, 3.4GHz speed with 2GB of Ram and a Windows XP operating system.

Initially, a larger step size was used with a simple Matlab interpolation filling in points between. It was found that the Matlab interpolation was smoothing out some of the frequency variation and distorting the time domain results. In the Gain vs frequency (20 MHz to 20 GHz) response plots of Figures 18 ands 19, some areas are circled showing the subtle variation that may not have been adequately represented by the simply interpolated data in Matlab. Further ongoing investigations will improve the interpolation methods which could be used to accurately represent the data with fewer simulated frequencies.

Figure 17 a) IRA Model Simulated Gain, b) IRA-2 Measured Gain [10, Figure 3.4]

12

Figure 18 IRA Simulated Frequency Response: a) unitless Gain, b) Magnitude

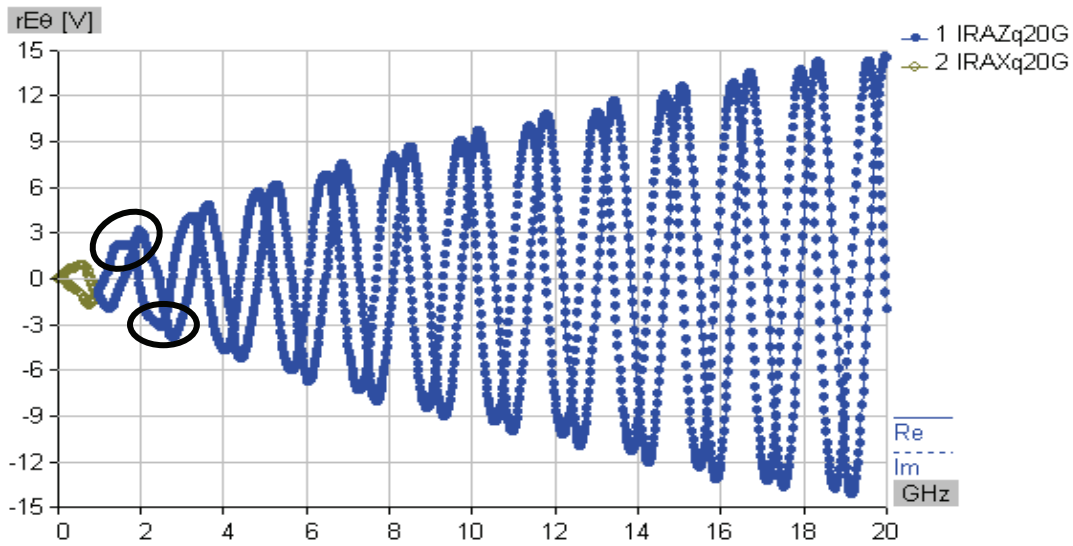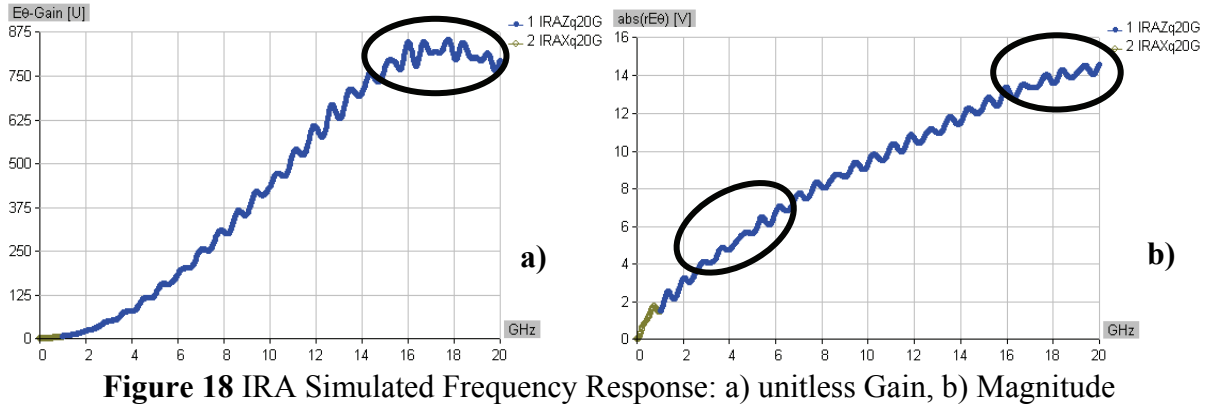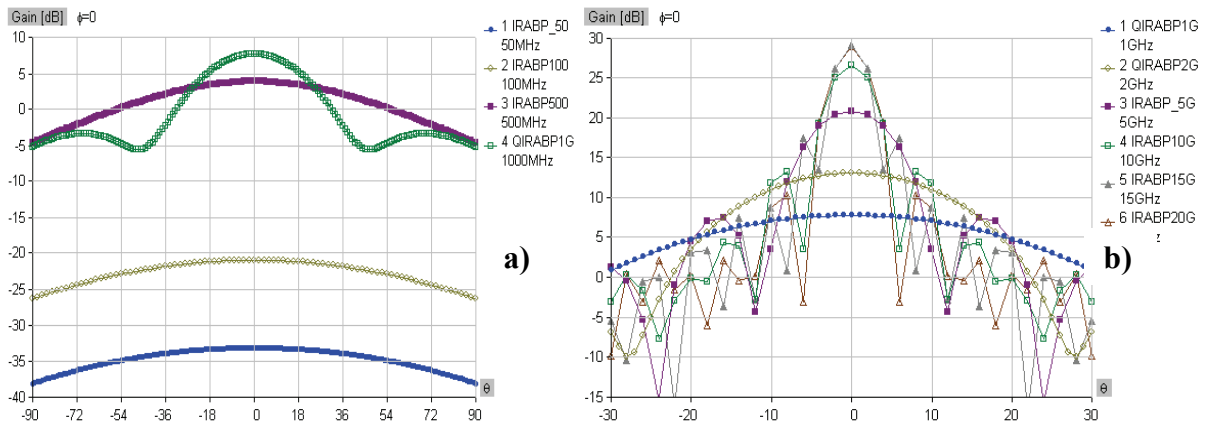**Figure 19** IRA Simulated Frequency Response, complex E_θ (real and imaginary)

Figure 20 shows the antenna pattern in the low frequency region (50, 100, 500 and 1000MHz) in Figure 20a and the pattern in the high frequency region (1, 2, 5, 10, 15 and 20GHz) in Figure 20b.

Figure 20 IRA Simulated Beam Pattern for a) low frequencies and b) high frequencies.

13

To transform Frequency Domain (FD) results simulated in WIPL-D to the Time Domain (TD), the process outlined below was followed. The process is described and accompanied by twelve plots of the radiation field analysis from FD to TD.

First, we bring the real and imaginary FD data set into Matlab and plot Figure 21a to verify agreement with WIPL-D data in Figure 19. The signal processing parameters selected and calculated for the analysis are summarized in Table 2 below. Next, we extend the length of the FD vector to N, insert the conjugate symmetric values and zero pad the remainder, which results in the plot shown in Figure 21b.

TABLE 2: List of signal processing parameters

| Parameter		Value	Description
Δf	set by simulation	20 MHz	frequency spacing or frequency resolution
N	select	$2^{11} = 2048$	sequence period (min 2 x no. of freq samples)
f_s	calc: $f_s = N\Delta f$	40.96 GHz	sampling frequency (duration of FD signal)
Δt	calc: $\Delta t = 1/ f_s$	24 psec	sampling interval or time resolution
T_0	calc: $T_0 = 1/\Delta f$	50 nsec	record length (duration of TD signal)
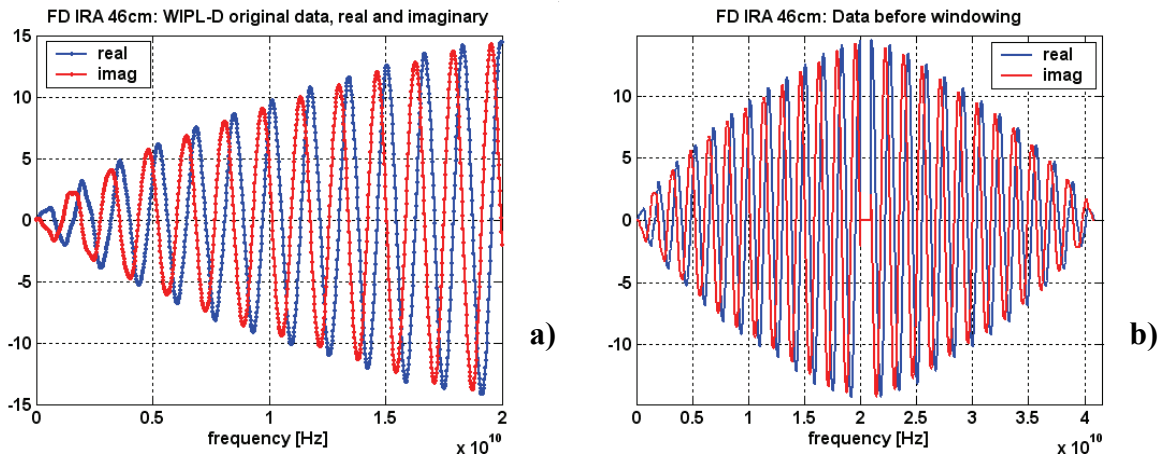
Figure 21 a) IRA Far-Field Radiation Real and Imaginary FD Data, compare to Figure 19
b) FD Real and Imaginary Data with Conjugate Symmetry and Zero Padding

We define a Gaussian pulse in the Time Domain and take the discrete Fourier transform (DFT) used to weight the FD data.

$$g(t) = e^{-\gamma^2}; \gamma = \frac{4}{T}(t - t_0), T = 0.25n\sec, t_0 = 5n\sec$$

The Gaussian Window is shown in Figure 22, with a width is approximately 16 GHz. The FD data is multiplied by the Gaussian Window, with the result plotted in Figure 23. Taking the Inverse Discrete Fourier Transform (IDFT) of this result gives the Far-Field Radiation Time Domain Signal, shown in Figure 24. To compare our results to theoretical and measured IRA responses using a step input, we integrate the time domain results, since the integral of the impulse gives the step function. The resulting plots in Figure 25 show the expected features, as discussed at the beginning of this section, including Figure 25c which demonstrates the derivative relationship between the time domain transmission and reception waveshapes.

14

Figure 26 shows the pulse and step input results overlaid and is the same as shown at the beginning, except without the Gaussian Pulse.
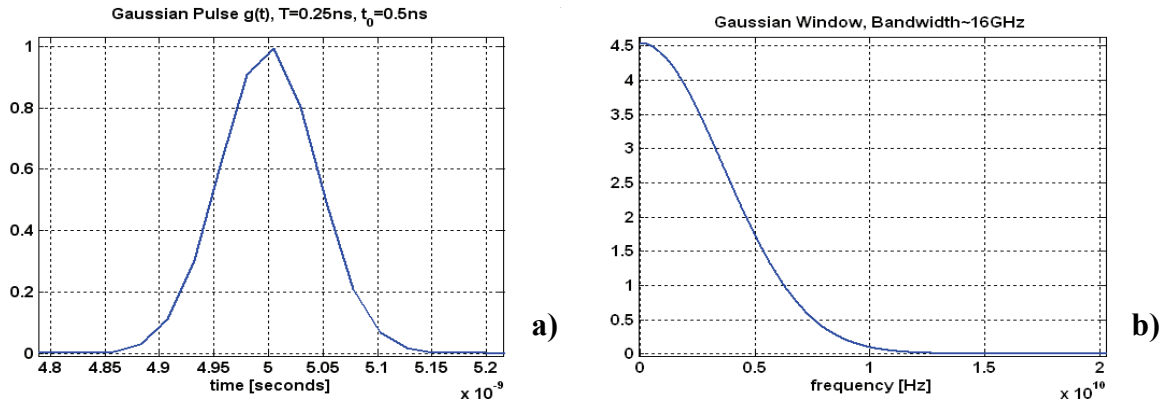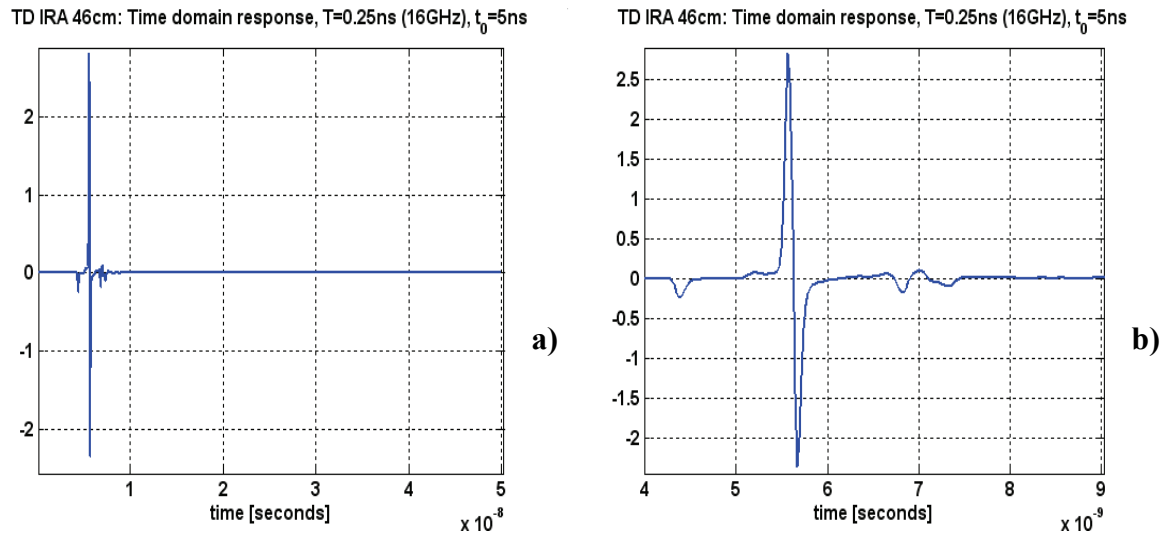

Figure 22 The Gaussian Window a) Time Domain g(t), b) Frequency Domain G(f)
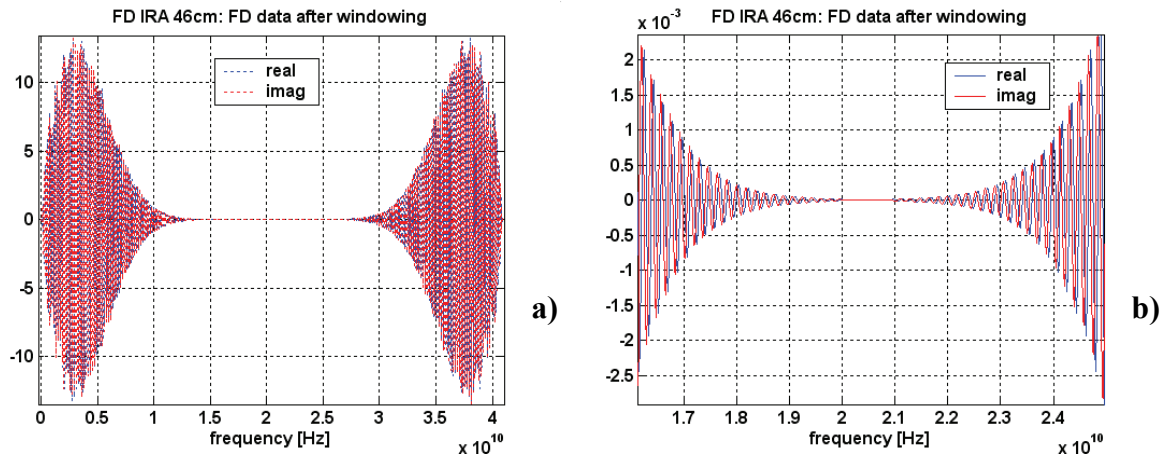
Figure 23 The Windowed FD data, before IDFT: a) full extent, b) zoom in around 20 GHz

Figure 24 The Far Field Radiation Time Domain: a) full extent, b) zoom in for signal features
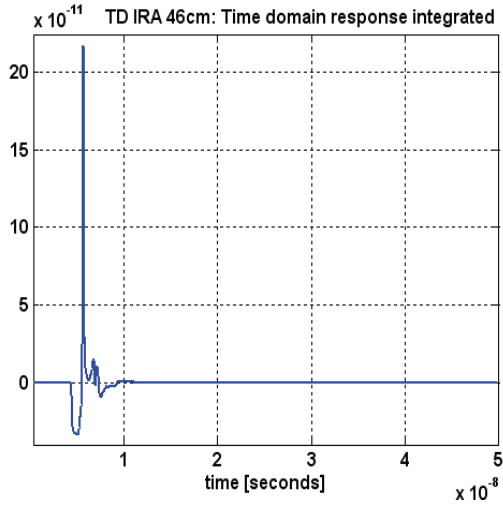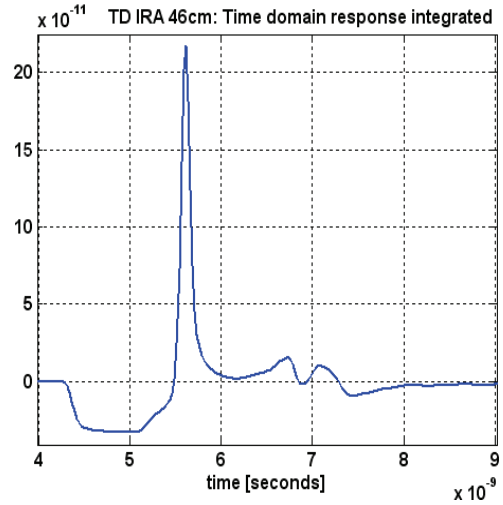
Figure 25 Integrated TD to Simulate a Step Input: a) full, b) zoom in for signal features
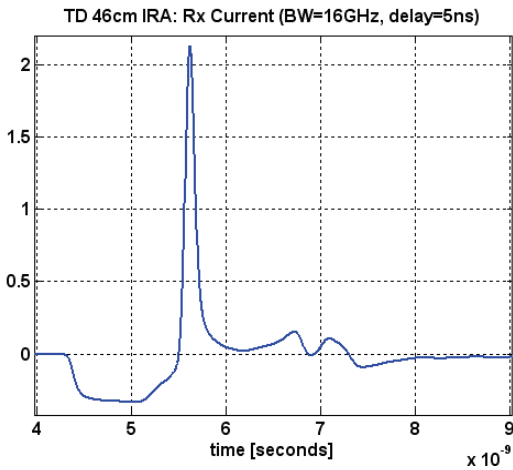
Figure 25 c) This plot of the received current due to an incident Gaussian pulse on the 46cm IRA demonstrates the expected derivative relationship between the transmit and received far field responses. The time domain response on reception is proportional to the integral of the time domain far field transmission.
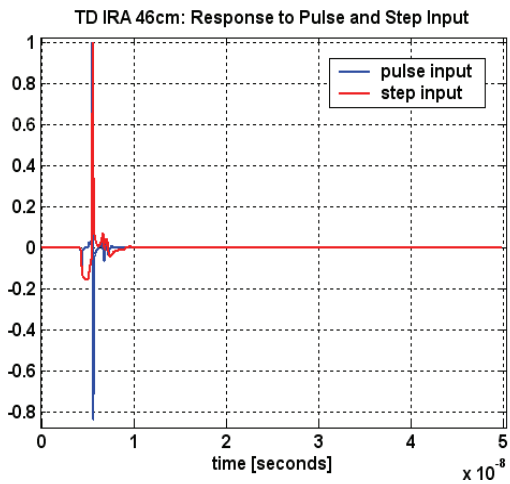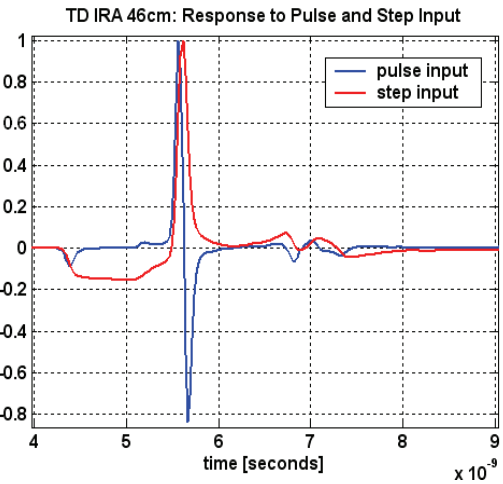
Figure 26 Far-Field Radiation with Pulse and Step Input: a) full, b) zoom in for features

16

b

DYNAMIC INPUT RESISTANCE OF THE IRA:

In this section, we calculate the dynamic input resistance of the 46cm diameter IRA in the frequency domain and then take the inverse discrete Fourier transform of the data to obtain the dynamic input resistance of the antenna. In Figure 27a, the blue line shows the transient input resistance or equivalently the dynamic resistance, $\mathfrak{z}_{11}(t)$, after it has been transformed from the frequency to the time domain by using the IDFT, with a simulated Gaussian impulse input.

To compare the simulated input impedance results to the IRA TDR measurements by E. Farr [4, 10], the time domain response is integrated. Integration of the results from an impulse input gives the response as if the input had been a step function. The red line in Figure 27a plots the integrated response. The shape of it is similar to the figures in [4, 10], recognizing that there is no cable length or signal splitters in the simulated model. The calculated time from the feed point along the feed arm to the resistors at the rim of the dish is L_a/c + wire lengths (feed + connector)/c = 1.16nsec, which is indicated on Figure 27a. The shape of the plots in Figure 27a is reasonable, and the amplitudes have been normalized to allow them to be viewed together. Figure 27b is a plot of Farr's IRA-2 measured TDR, shown for reference to compare to the shape of the red line in Figure 27a [10, Figure 3.2].
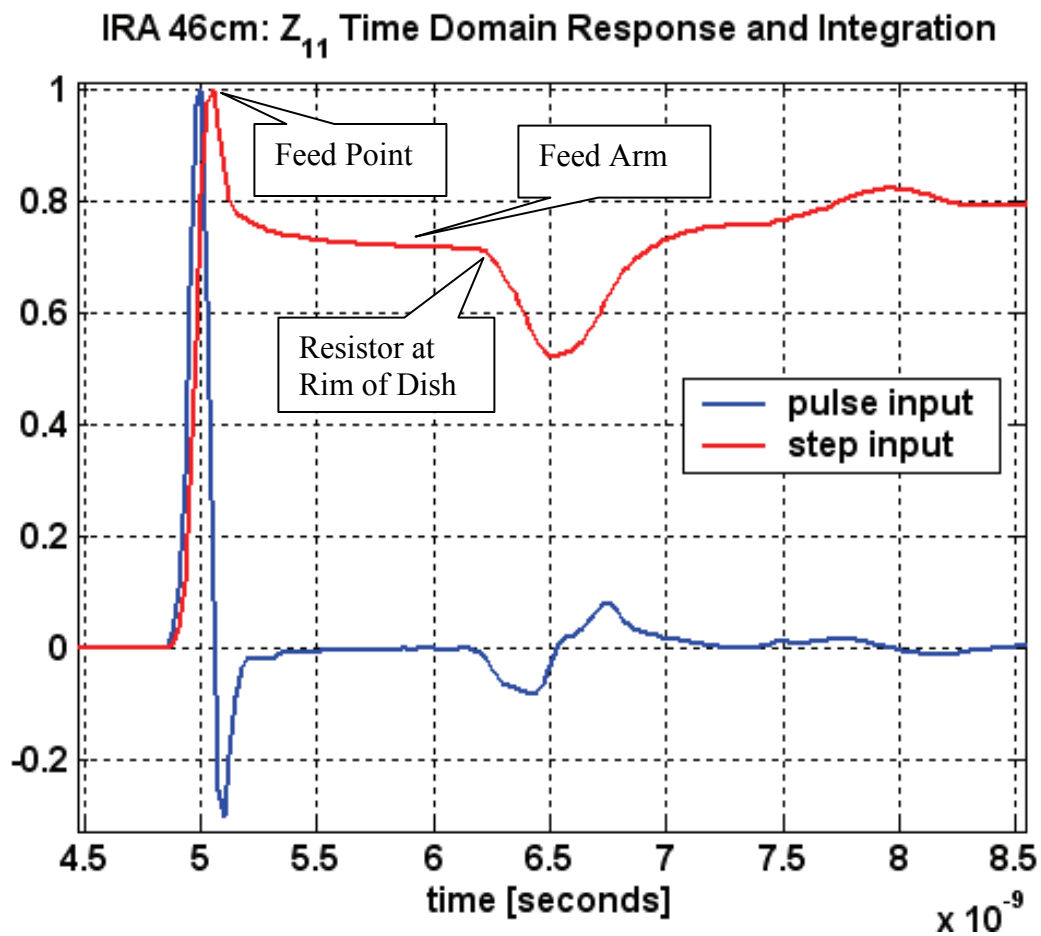

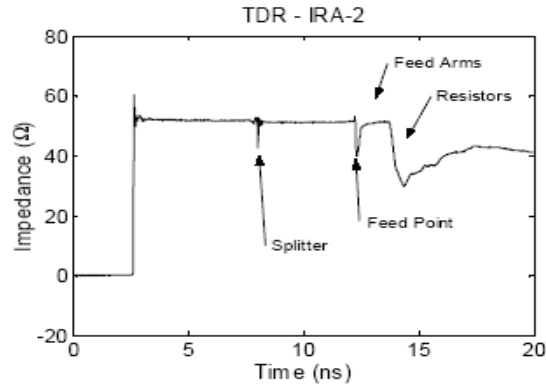**Figure 27** a) IRA Model Simulated Dynamic Resistance

17

Figure 3.2. TDR of the IRA-2.

Figure 27 b) IRA-2 Measured TDR [10, Figure 3.4]

The variation of the Input Impedance Z_{11} as a function of frequency is shown in Figure 28 below. The impedance data has been computed using the same quarter symmetric model and simulation which gave the radiation data. The number of unknowns was 2583 and the parameters used in the simulation are the same as the previous analysis.

The WIPL-D plot of the real and the imaginary parts of the input impedance is shown in Figure 29 to produce the complete IRA frequency response from 20 MHz to 20 GHz, with a 20 MHz step size. Several of the plots overlay an additional project titled "46t2R200" which shows the same 46cm, quarter symmetric IRA performance with a 200Ω load resistance. It is interesting to note that there are small differences in the values of the input impedance in Figure 30 of the IRA, when WIPL-D automatically discretizes the structure at the highest frequency of interest which in one case was 2 GHz and for the other case was 20 GHz. Clearly, discretizing the IRA for 20 GHz requires more unknowns than the simulation to 2 GHz.

Plots of the input reflection coefficient S_{11} are shown in Figure 31 as it is a critical performance parameter influenced by the antenna impedance primarily at low frequencies.
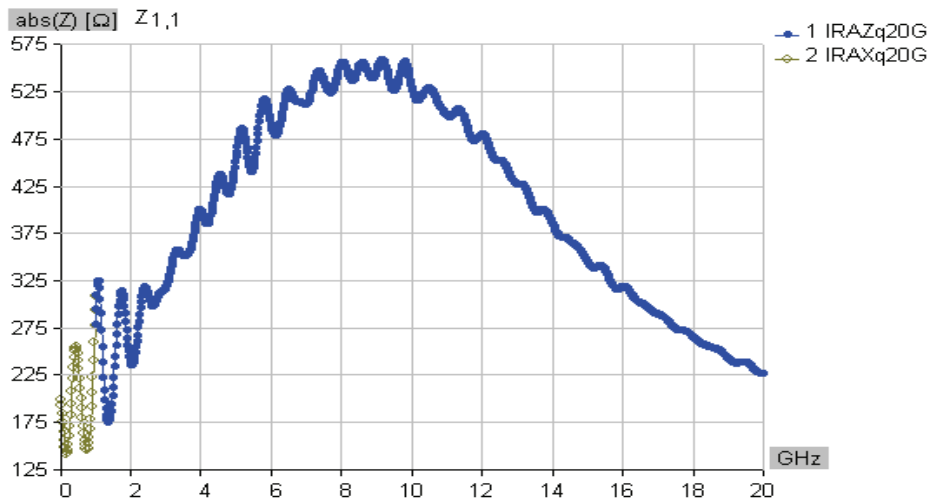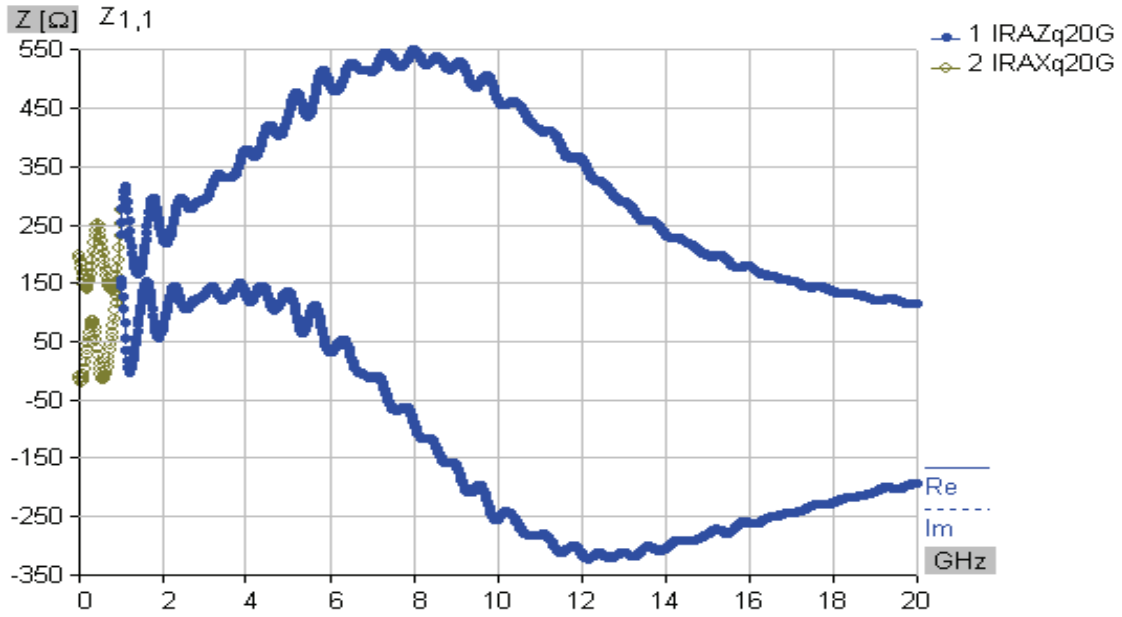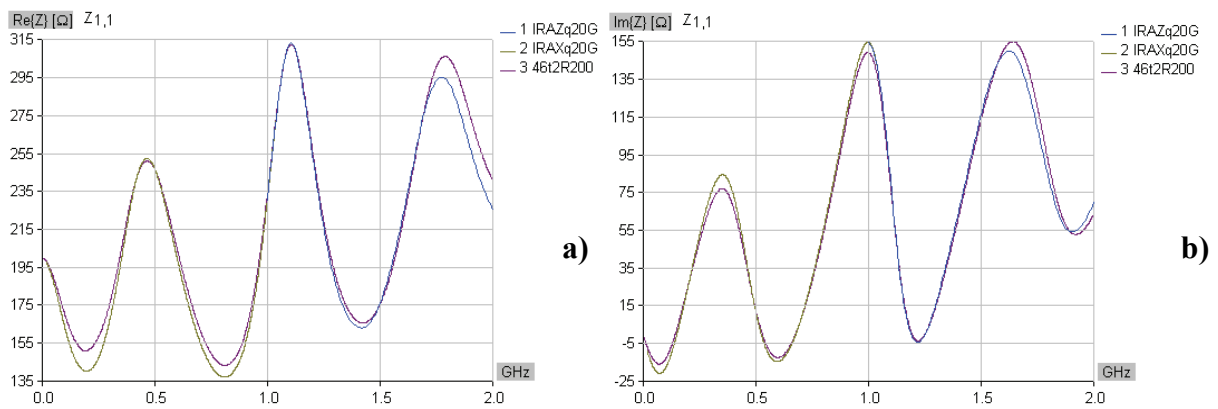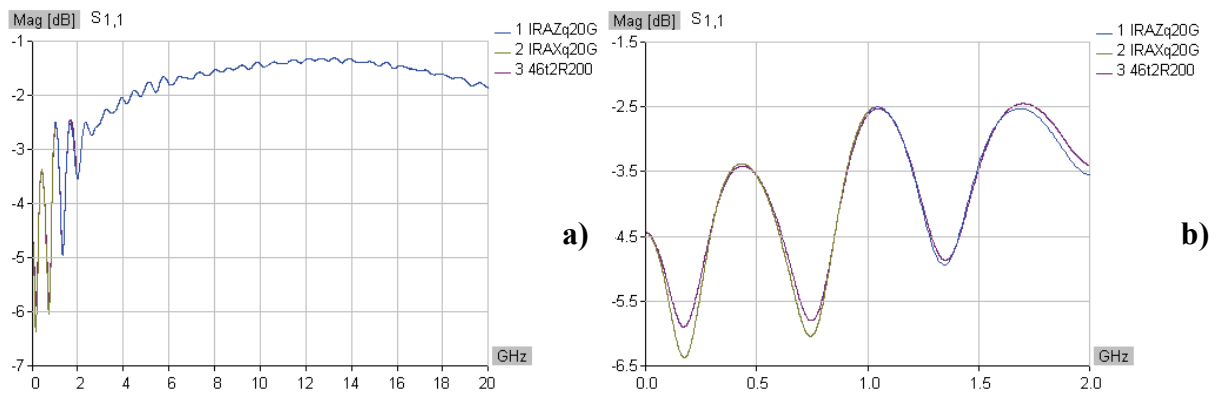

Figure 28 IRA Frequency Response, Z_{11} Magnitude

18

Figure 29 IRA Input Impedance vs. Frequency, Complex Z_{11} (real and imaginary)

Figure 30 IRA Complex Input Impedance, zoom in on 2GHz, Z_{11}: a) Real, b) Imaginary

Figure 31 IRA Input Reflection Coefficient, S_{11}: a) full bandwidth, b) zoom in on 2GHz

To transform Frequency Domain (FD) results simulated in WIPL-D to the Time Domain (TD), the same process outlined in the previous radiation results section was followed. The process is briefly repeated and accompanied by ten plots of the input impedance analysis.

In the far field radiation case, the zero frequency point is set to zero for the time domain analysis, since there is no radiation at DC. For the impedance case, the zero frequency point was set to 200Ω for the real part and zero for the imaginary part of the complex impedance data. This corresponds to the conclusion that a DC current would see the load impedance value as the input impedance.

As before, we first transport the real and imaginary FD impedance data set into Matlab and obtain the plot in Figure 32a. The signal processing parameters selected and calculated for the analysis are the same ones as before, summarized previously in Table 2. Next, we extend the length of the FD vector to N, insert the conjugate symmetric values and zero pad the remainder to result in the plot of Figure 32b.

The same Gaussian weighting shown in Figure 22 is used to modify the FD data and obtain the windowed FD data shown in Figure 33. The Inverse Discrete Fourier Transform (IDFT) of this convolution in frequency gives the dynamic input resistance in Figure 34.

To compare our results to the theoretical and measured IRA responses using a step input, we integrate the time domain results, since the integral of the impulse gives the step function. The displays then approximate the Time Domain Reflectometer (TDR) plots in the references [3, 4]. Figures 35 and 36 show the expected features, as discussed at the beginning of this section. The final plots shown are the same shown at the beginning, with the amplitude normalized.
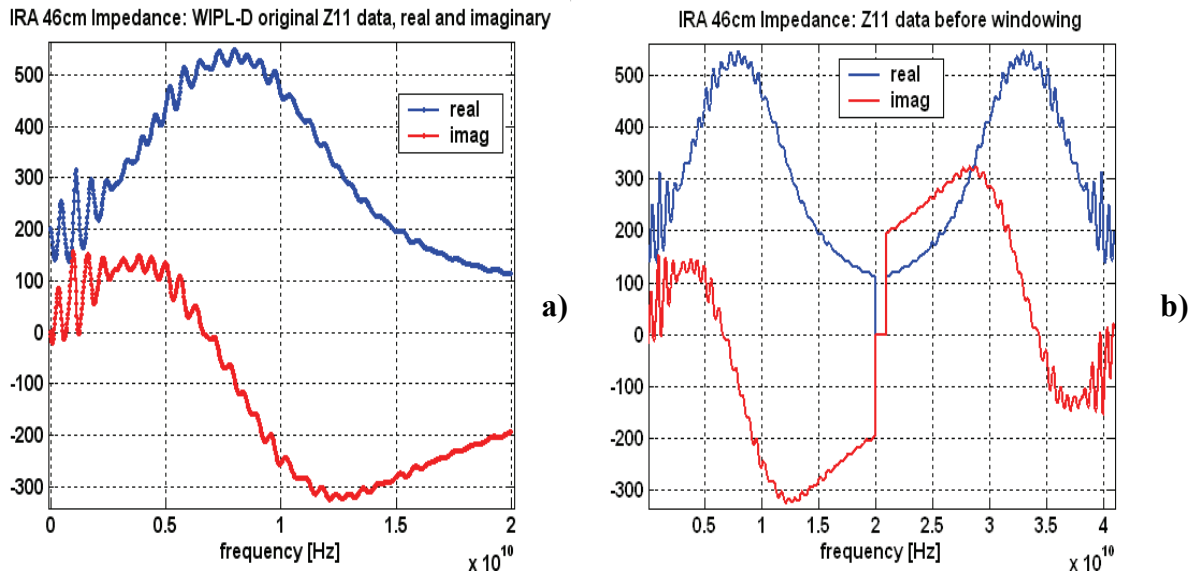
Figure 32 a) IRA Input Impedance Real and Imaginary FD Data, as compared to Figure 29
b) FD Real and Imaginary Data with Conjugate Symmetry and Zero Padding.

20
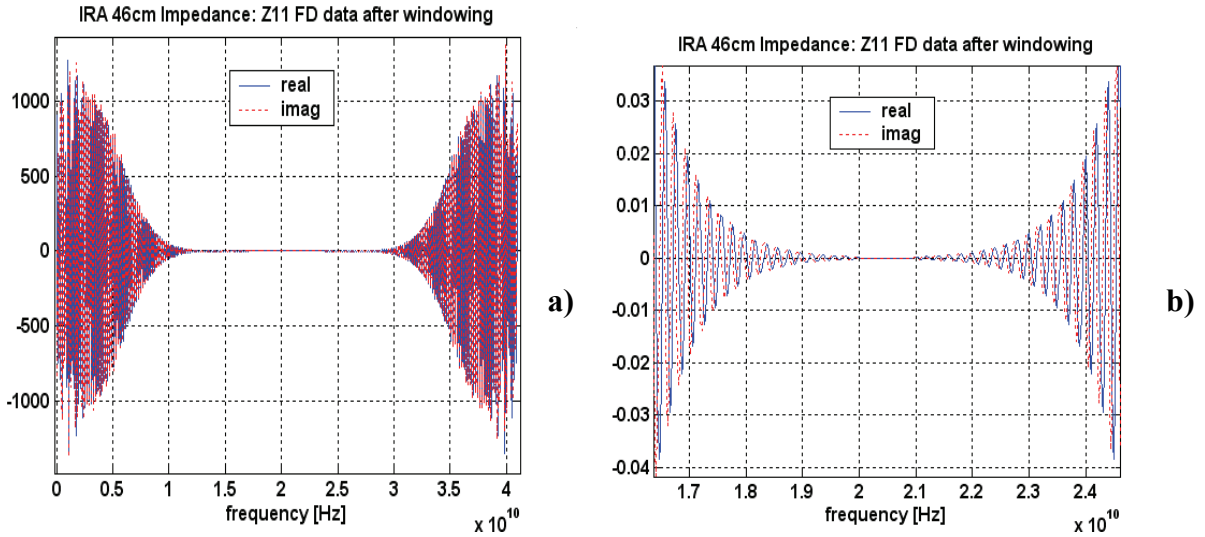
Figure 33 The Windowed FD data, before IDFT: a) full extent, b) zoom in around 20 GHz
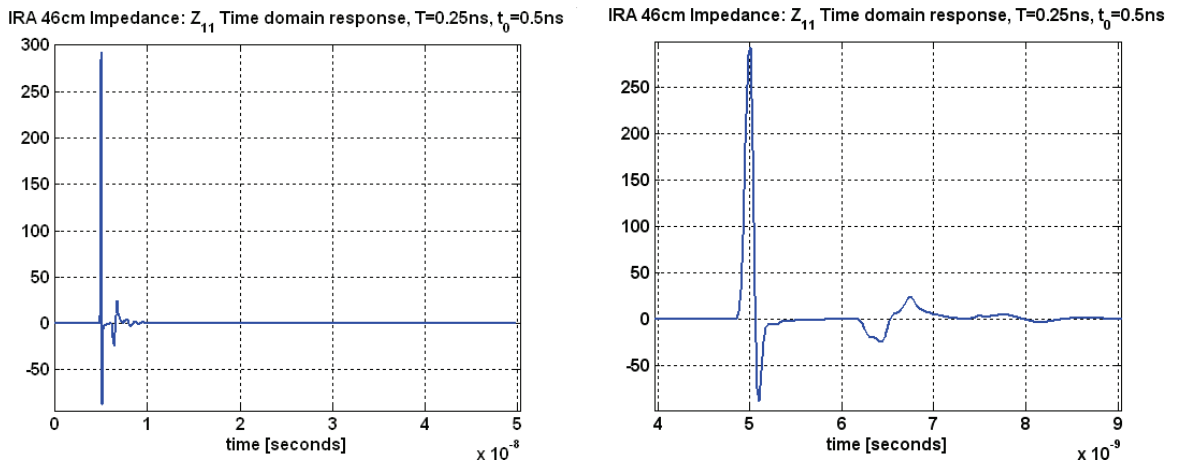
Figure 34 The Dynamic Resistance, pulse input: a) full extent, b) zoom in for signal features
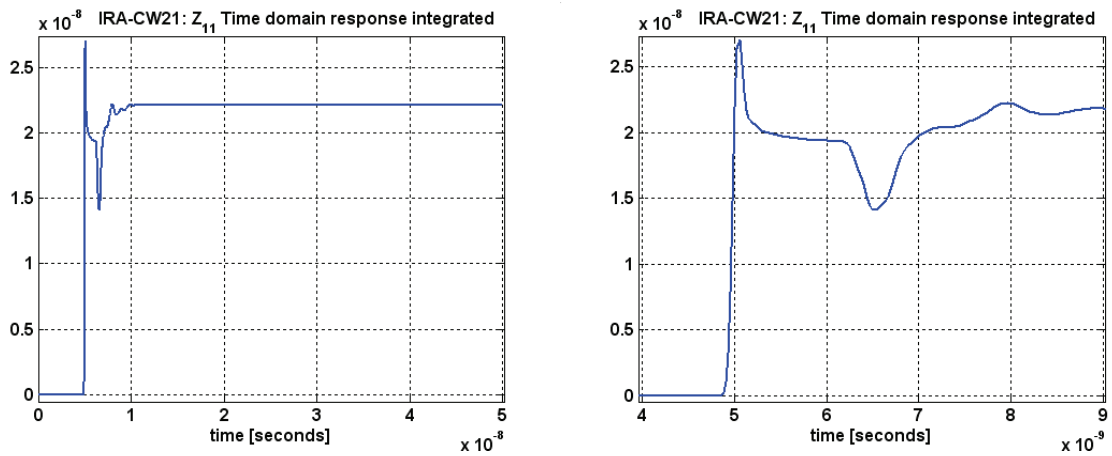
Figure 35 Step Input Provides TDR Result: a) full extent, b) zoom in for signal features

Figure 36 Input Impedance with Pulse and Step Input: a) full extent, b) zoom in for features

A STUDY OF THE VALUE OF THE LOAD RESISTANCE IN THE FEED ARMS OF THE 46cm DIAMETER IRA:

Next we investigate the effect in far field pattern of the IRA on the choice of the resistance connecting the feed arms of the IRA to the reflector. It is seen from the numerical simulations of the far field of the IRA by using WIPL-D that the choice of the 200Ω resistance in the feed arm appears to be an excellent s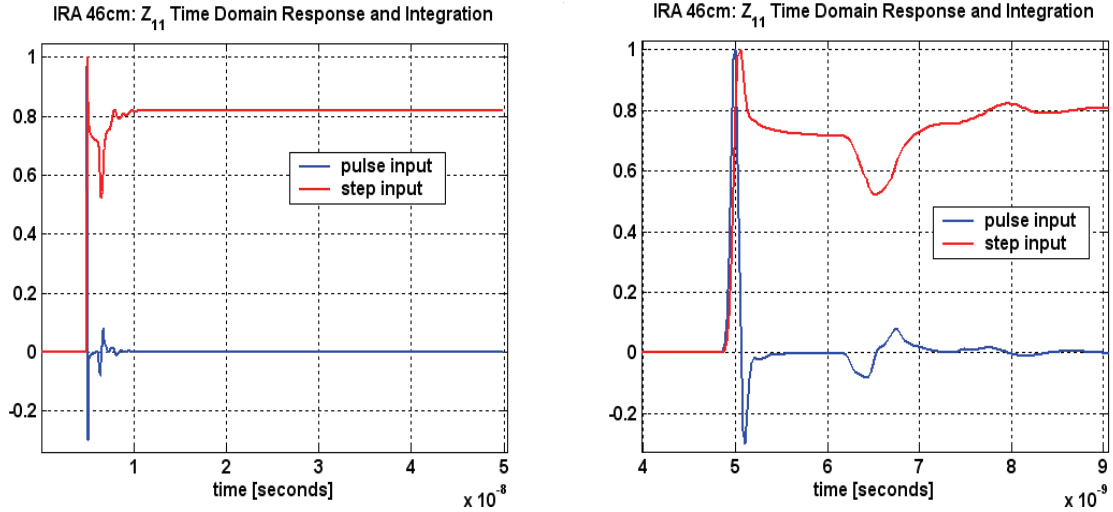election. This is illustrated through the plots in Figures 37-42. Initially, an optimization routine using the WIPL-D tool, was executed to evaluate the optimum value of the resistance. That yielded 557Ω, when optimization was based on far field radiation alone. Additional work can be done with the tool, factoring in the impact of input reflection coefficient and focusing on the low band of frequencies.

However, based on the initial results, a study was made running several projects for the frequency response for different values of the resistance, up to 600Ω. The plots that follow overlay the results obtained using seven different values of the load resistance 0, 50Ω, 100Ω, 200Ω, 400Ω, 500Ω, 600Ω, for comparison. Figure 37 provides the response up to 20 GHz, whereas Figure 38 shows the results over only half the frequency range and Figure 39 zooms in to 2GHz frequency range. Figure 37 illustrates that if there is no load then the performance is poor. As expected, having no load resistance is unacceptable, and this case will not be shown in later figures. The results have been generated using the quarter symmetric model of the IRA and the results have been computed at 400 frequency points with a 5MHz step size. From Figure 39, it appears that the choice of 200Ω (blue line) or 100Ω (purple line) generate similar and acceptable results. Figure 40 shows the same plot to up to 0.7 GHz, and shows that 200Ω is the superior selection for 2dB higher gain. These figures verify that, as expected, the load resistance has an effect primarily at the lower end of the frequency range.

22

Poor Performance with No Resistance in the Feed Arms
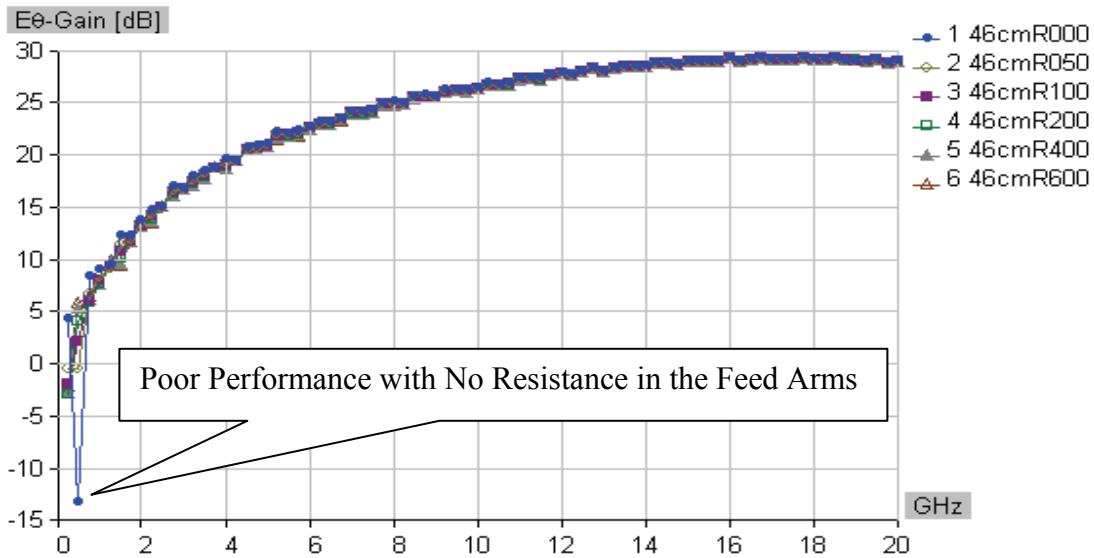
Figure 37 plots the gain of the IRA as a function of frequency for different values of the resistance in the feed arm. Six different load resistors are compared: 0, 50Ω, 100Ω, 200Ω, 400Ω, 600Ω.
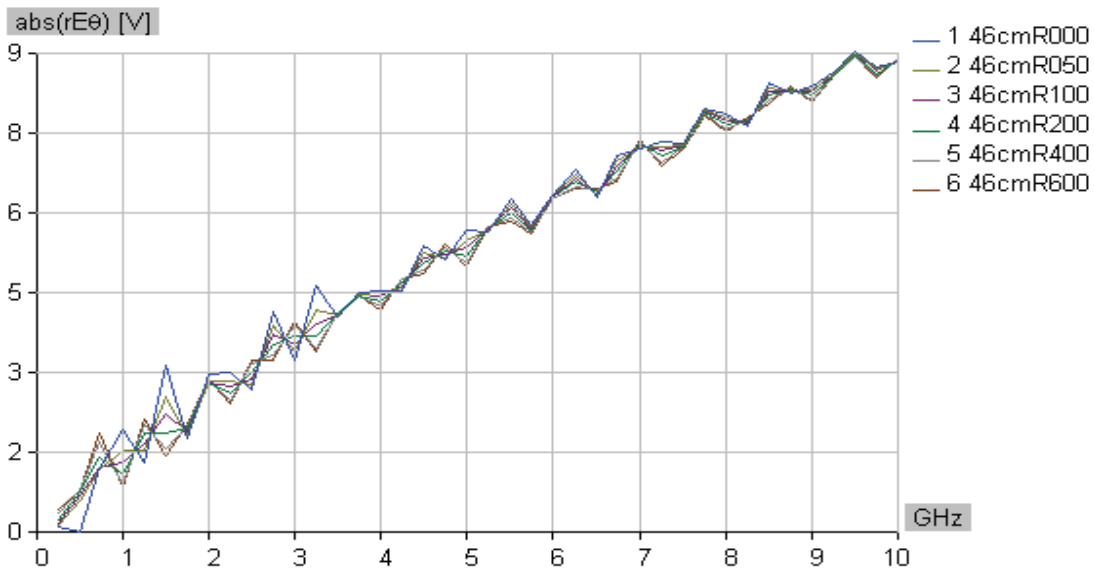
Figure 38 plots the far field of the IRA as a function of frequency to up to 10 GHz for different values of the resistance in the feed arm. Six different load resistors are compared: 0, 50Ω, 100Ω, 200Ω, 400Ω, 600Ω.
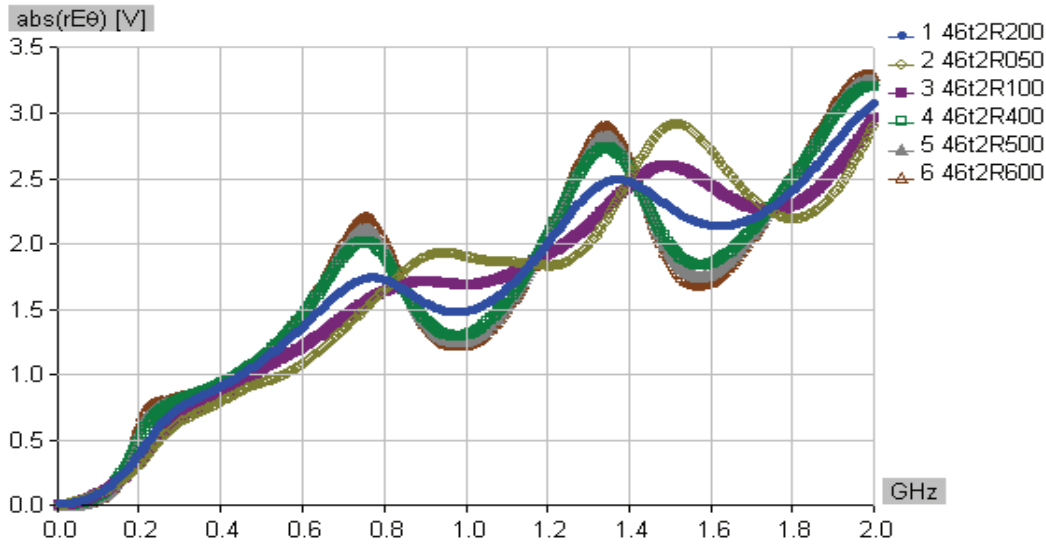
Figure 39 plots the far field of the IRA as a function of frequency, focusing in on the low frequencies up to 2GHz. Six different load resistors are compared: 50Ω, 100Ω, 200Ω, 400Ω, 500Ω, 600Ω.

From Figure 39, it appears that a 200Ω (blue line) or 100Ω (purple line) give similar acceptable results. However, the next plot, Figure 40, zooms in on a section near the knee of the dB Gain plot of the same data, which clearly shows that the 200Ω (blue line) load resistor is a better choice giving about 2dB higher gain at 500MHz than the 100Ω (purple line).
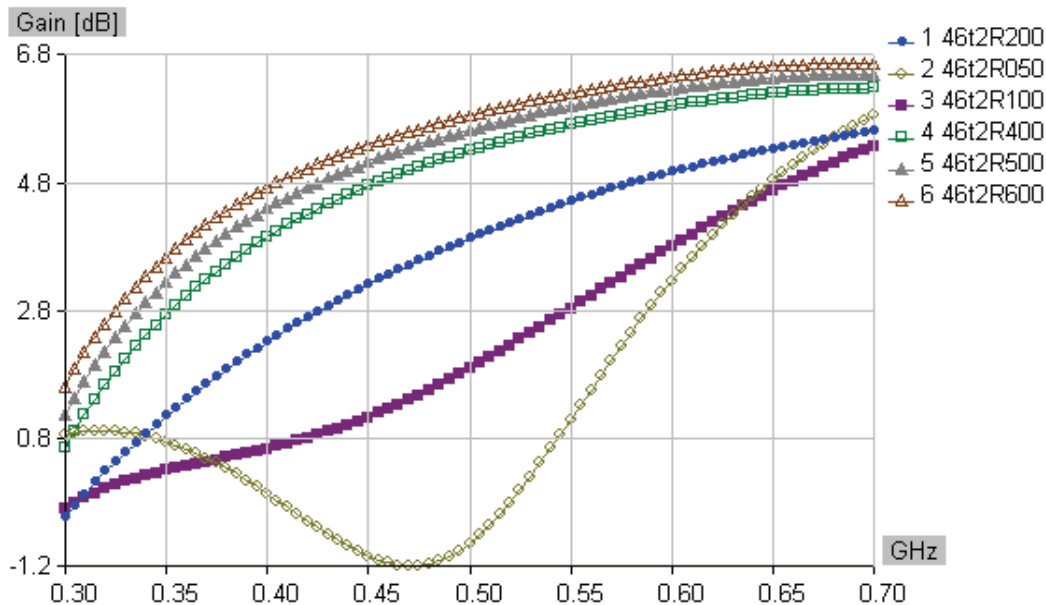

Figure 40 plots the dB gain of the IRA as a function of frequency up to 0.7 GHz for the different values of the resistance in the feed arm. Six different load resistors are compared: 50Ω, 100Ω, 200Ω, 400Ω, 500Ω, 600Ω.

24

The connecting load resistance also influences the variation of the input impedance of the IRA. This will affect the input return loss or the input reflection coefficient, S_{11}. Figure 41 plots the variation of S_{11} over a bandwidth of 2GHz as a function of the six different values of the connection resistance. Again, it appears that 200Ω offers the most consistent performance.
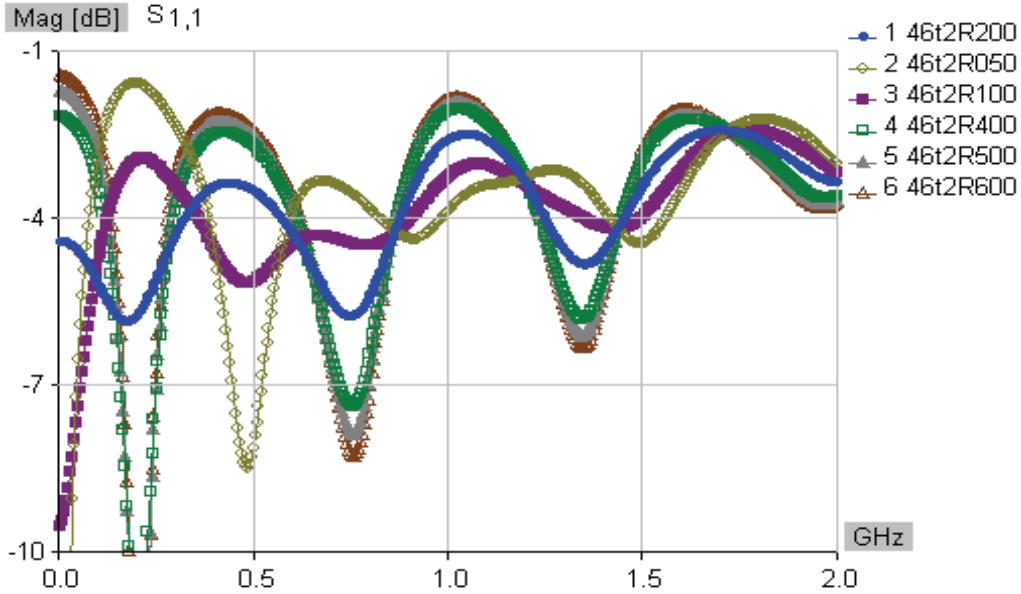
Figure 41 plots the scattering parameter S_{11} to illustrate the input impedance match over the low end of the frequency band of interest. Six different load resistors are compared: 50Ω, 100Ω, 200Ω, 400Ω, 500Ω, 600Ω.
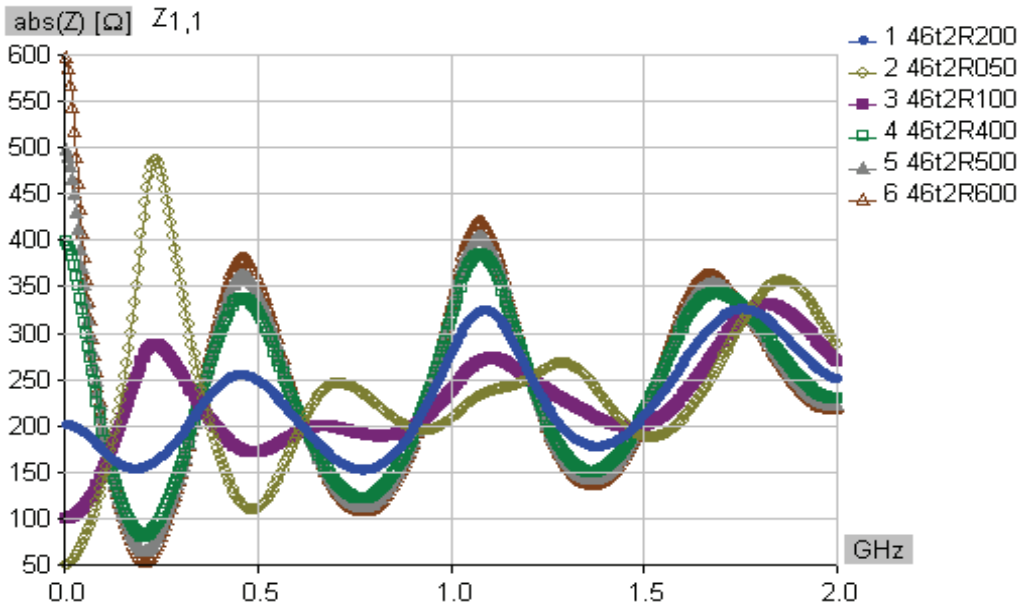
Figure 42 plots magnitude of the input impedance of the IRA as a function frequency for the different values of the resistance used in the feed arm. Six different load resistors are compared: 50Ω, 100Ω, 200Ω, 400Ω, 500Ω, 600Ω.

25

Figure 42 shows the magnitude of the input impedance of the IRA up to 20GHz as a function of the connecting load resistance. Again it is clear that 200Ω is a good choice. This last plot of impedance vs. frequency shows the magnitude Z_{11} for the six different load resistance values. Figure 42 is interesting because it shows that each different load resistor plots tends to a unique resistor value at the low frequency end of the spectrum. This is the case since the load impedances at the ends of each pair of feed arms, which are in parallel, will add as resistors in parallel and result in an equivalent resistance of half the load impedance of one arm. A current from the feed wire, through one pair of the feed arms and across the reflector, will then see the equivalent resistance of the other pair of feed arms. These two equivalent resistances will add as resistors in series and sum to the initial value of load resistance. Therefore, that is the value each plot tends toward at the low frequency, which is the value that a DC current would see.

CONCLUSION:

The description and plots provided here illustrate that it is possible to duplicate measured results both in the time and frequency domain of the electrical characteristics of a complex antenna using an electromagnetic analysis code. Using WIPL-D, we have modeled and simulated an IRA based on a Farr Research 46cm diameter IRA with 45º feed arms. We analyzed the results to obtain the time domain response by weighting the frequency domain data by a Gaussian window and using inverse discrete Fourier transform (IDFT) through Matlab. To compare to the step input results obtained by Farr research, we integrated the time domain response due to our impulse input so as to obtain the step response of the IRA. The results compare favorably to Farr's measured results [3,4] and Baum's theoretical description [9]. To compare to the TDR results obtained by Farr research, we integrated the dynamic input resistance time domain response resulting in an equivalent response that would be obtained by a time domain reflectometer (TDR). Again, the shape of the resulting plot is similar to results published by Farr, from the feed point to the reflector rim. We presented plots comparing six values of the resistance in the feed arms and conclude that the 200Ω selection provides the best balance between competing design parameters at low frequencies. Additional work placing the modeled structures into radiation and scattering scenes shows promise in further efficiency and simplification of the iterative process of measurement and design optimization.

REFERENCES:

[1] E. G. Farr, L. H. Bowen, G. R. Salo, J. S. Gwynne, C. E. Baum, W. D. Prather and T. C. Tran, "Studies of an Impulse Radiating Antenna and a Pulse Radiating Antenna Element for SAR and Target Identification Applications", Sensor and Simulation Note 442, March 2000.
[2] L. H. Bowen, E. G. Farr, C. E. Baum, T. C. Tran and W. D. Prather, "Experimental Results of Optimizing the Location of Feed Arms in a Collapsible IRA and a Solid IRA", Sensor and Simulation Note 450, November 2000.
[3] E. Farr, "IRA-2 Dimensions", Farr Research, Inc. document dated March 15, 2000. This document is provided with minor edits in the Appendix for reference.

[4] E. Farr, "Analysis of the Impulse Radiating Antenna", Farr Research, Inc., Sensor and Simulation Notes 329, July 1991.

[5] K. Kim and W. R. Scott, Jr., "Numerical Analysis of the Impulse-Radiating Antenna", Sensor and Simulation Note 474, June 2003.

[6] D. V. Giri, H. Lackner, I. D. Smith, D. W. Morton, C. E. Baum, J. R. Marek, W. D. Prather and D. W. Scholfield, "Design, fabrication, and testing of a paraboloidal reflector antenna and pulser system for impulse-like waveforms", IEEE Trans. Plasma Sci., Vol. 25, No. 2, pp. 318-326, Apr 1997.

[7] L. H. Bowen, E. G. Farr, D. I. Lawry, "A Dual-Polarity Impulse Radiating Antenna", Sensor and Simulation Note 479, October 2003.

[8] B. M. Kolundžija, J. S. Ognjanović and T. K. Sarkar, "*WIPL-D* (for Windows manual)", Artech House, Norwood, Mass. 2000 (http://wipl-d.com).

[9] C. E. Baum and E. G. Farr, "Impulse Radiating Antennas", in H. L. Bertoni (eds.), pp. 139-147 in *Ultra-Wideband, Short-Pulse Electromagnetics*, New York, Plenum, 1993.

[10] L. H. Bowen, E. G. Farr, C. E. Baum, T. C. Tran and W. D. Prather, "Results of Optimization Experiments on a Solid Reflector IRA", Sensor and Simulation Notes 463, January 2002.

[11] J. S. Tyo, "Optimization of the TEM Feed Structure for Four-Arm Impulse-Radiating Antennas", IEEE Trans. on Antennas and Propagation, Vol 49, No 4, pp 607-614, April 2001.

Farr
Research, Inc.

IRA-2 Dimensions
Everett Farr
March 15, 2000

Feed Arm for specified IRA
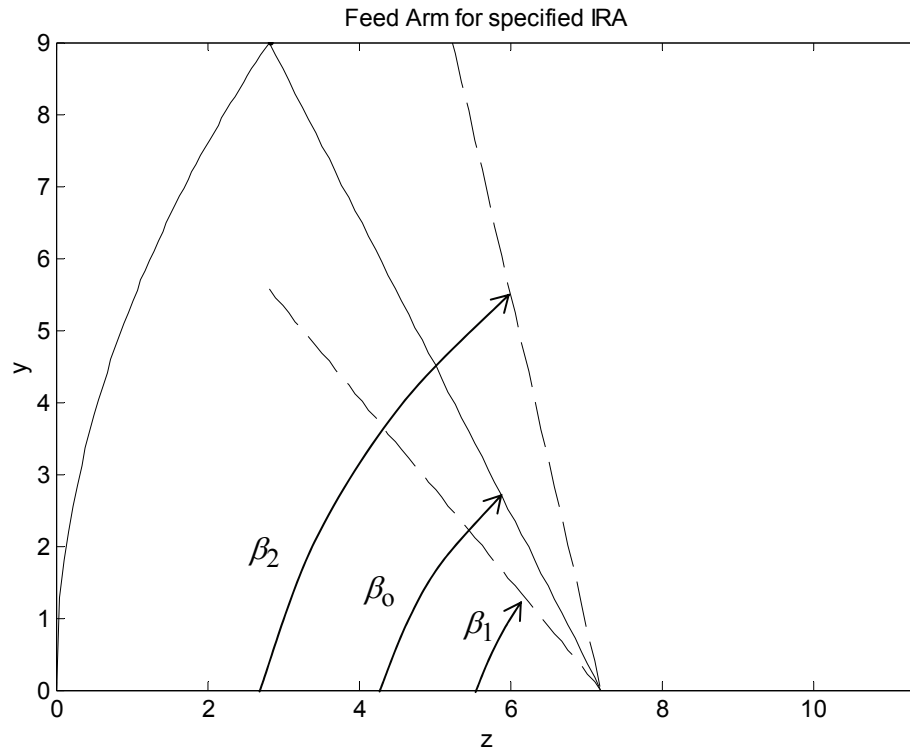
Above is a slice through one of the feed arms.

Dimensions are as follows:

radius =   9.000 inches
focus =   7.200 inches
depth =   2.813 inches
focus to rim = 10.012 inches

beta1 = 51.747 degrees
beta0 = 64.011 degrees
beta2 = 77.697 degrees
beta2-beta1 = 25.950 degrees

The four feed arms are positioned at ±30° to a vertical line, when the antenna is oriented for vertical polarization. The feed arms are perfect triangles out to a distance of one focal length, where they terminate to the edge of the dish in 200 Ω resistors. The feed arms are normally fabricated from flat plate stock that is 0.060 inches thick.

The antenna is fed with a differential feed, with the top two arms positive and the bottom two arms negative.

The antenna is normally driven by a band-limited step function. The radiated waveform is an approximate derivative of the driving voltage, or an approximate impulse.

The details of some of the plastic structural support near the focus can be added that later if the modeling and simulation is successful.

The placement of the resistors at the end of the feed arms can be seen in the photo below. The feed arms are anchored to the reflector with G10 circuit board. Each arm has 2 strings of resistors in parallel to the reflector, and each string is 400 ohms. So each arm has 200 ohms to ground, providing a matched impedance.

This recent design includes a ground plane that lies in a plane of symmetry, and does not affect the antenna.